Aligned ZnO Nanorods with Tunable Size and Field Emission on Native Si Substrate Achieved via Simple Electrodeposition

Zhuo Zhang,[†] Guowen Meng,*[,†] Qiaoling Xu,[†,‡] Yemin Hu,[‡] Qiang Wu,[‡] and Zheng Hu*[,‡]

Key Laboratory of Materials Physics, and Anhui Key Laboratory of Nanomaterials and Nanostructures, Institute of Solid State Physics, Chinese Academy of Sciences, Hefei 230031, People's Republic of China, and Key Laboratory of Mesoscopic Chemistry of MOE, School of Chemistry and Chemical Engineering, Nanjing University, Nanjing 210093, People's Republic of China

Received: September 9, 2009; Revised Manuscript Received: October 19, 2009

Large-scale arrays of aligned ZnO hexagonal nanorods with planar ends have been achieved on a bare native *n*-type (100) Si substrate via a simple electrochemical deposition in $Zn(NH_3)_4(NO_3)_2$ solution with a pure Zn sheet as the anode without using any catalysts, additives, and additional seed crystals. The ZnO hexagonal nanorods grow from the single-crystal seeds self-formed in the initial stage of the electrochemical deposition. The diameters and the lengths of the ZnO nanorods can be tailored by adjusting the electrolyte concentration and the electrodeposition duration. Field-emission measurements show that the ZnO nanorods with smaller diameters exhibit lower turn-on field and higher current density. The well-aligned ZnO hexagonal nanorods (on Si substrate) with tunable size and field emission performance may have potentials in the future of nanotechnology.

1. Introduction

One-dimensional (1D) ZnO nanostructures have received much attention due to their potential applications in nanogenerators,[1,2] UV lasers,[3] light-emitting diodes,[4,5] sensors,[6] and field-emission devices.[7,8] Up to now, various synthetic approaches have been developed for 1D ZnO nanostructures, mainly including chemical vapor deposition (CVD),[9,10] metal-organic CVD,[11,12] pulsed laser deposition,[13] hydrothermal synthesis,[14] and electrochemical deposition.[15] Gas-phase approaches usually have lower product yield[16] and require specific substrate and laboratory apparatus operating at high temperatures. Comparatively, solution-phase approaches have many advantages, such as high yield of products, low-temperature, and optional substrate.[17] For example, hydrothermal and sonochemical methods have been used to prepare well-aligned ZnO nanorods.[18,19] However, these nonelectro solution-phase approaches require pressure-resistant equipment, and the motivities derived from gravity, thermal convection, or ultrasonic cavitation reduce the morphology controllability of the nanostructures.[20] All these could be overcome by using electrochemical deposition method. For instance, crystalline ZnO nanotubes were produced via template-assisted electrodeposition,[21] and precisely positioned and spatially separated ZnO nanorod arrays were synthesized on patterned substrate by electrodeposition.[22] Although the orientation, morphology, and crystallinity of the ZnO nanostructures are effectively improved under the applied electric field, the use of complex solutions or buffer layers makes the whole fabrication process complicated.[23] Therefore, exploring a simple, catalyst-free, and nonbuffer-layer method for large-scale arrays of ZnO nanorods with tunable size and property still remains a great challenge.

Here, we demonstrate a very simple and efficient approach to large-scale aligned ZnO hexagonal nanorods with planar ends on native Si substrate. The ZnO nanorods were achieved via electrochemical deposition in $Zn(NH_3)_4(NO_3)_2$ solution where pure Zn serves as anode, without using any templates, catalysts, additives, and additional seed crystals or coating metal oxide layers. As arrays of 1D ZnO nanostructures are good candidates for field emission (FE) due to their thermal stability with melting point over 1000 °C,[24] oxide resistibility, and high aspect ratio,[25] we investigated the FE performance of the ZnO hexagonal nanorods with different sizes.

2. Experimental Section

The electrochemical deposition of the well-aligned ZnO hexagonal nanorods was performed in a simple electrochemical cell self-made from Teflon (see Figure S1 of Supporting Information). The electrochemical cell was put into a water bath at 80 °C during the whole electrodeposition. A pure Zn (99.99% purity) sheet acted as the anode and a piece of Si substrate was fixed tightly on the Cu cathode.

The electrolyte $Zn(NH_3)_4(NO_3)_2$ solution was prepared by gradually dropping ammonium hydroxide (28 wt % NH_3 in water, 99.99%) into zinc nitrate hexahydrate ($Zn(NO_3)_2 \cdot 6H_2O$, 98%) aqueous solution until the solution became clear, with a pH value of about 10.

The ZnO nanorods were characterized by using field-emission scanning electron microscopy (FESEM) (SIRION 200), transmission electron microscopy (TEM) (JEM-2010), and X-ray diffraction (XRD) (X'Pert Pro MPD).

3. Results and Discussion

FESEM observations (Figure 1a) reveal that large-area arrays of uniform ZnO nanorods with planar ends have been grown on the Si substrate. An enlarged top view (upper-right inset of Figure 1a) displays that the nanorods with planar ends are hexagonal prisms with six crystallographic planes connected

* To whom correspondence should be addressed. E-mail: gwmeng@issp.ac.cn (G.W.M.); zhenghu@nju.edu.cn (Z.H.).
† Chinese Academy of Sciences.
‡ Nanjing University.

10.1021/jp9087223
Published on Web 11/03/2009

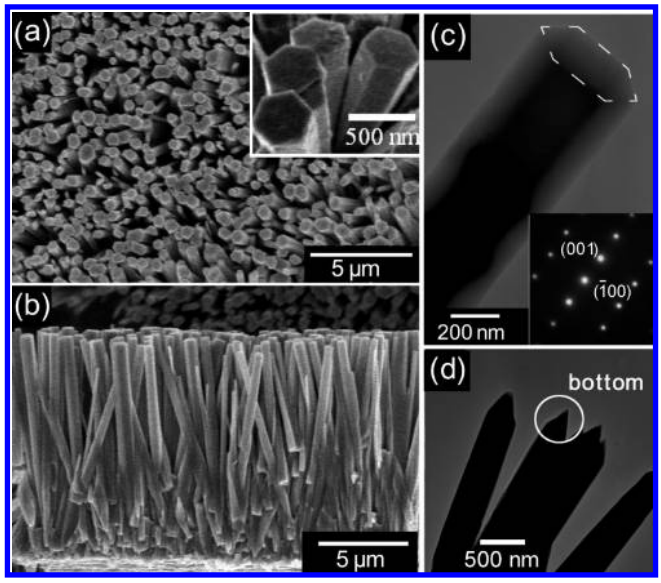

Figure 1. The aligned ZnO nanorod arrays electrodeposited from 0.5 M $Zn(NH_3)_4(NO_3)_2$ solution for 5 h. (a) Top-view SEM images (the inset is a close-up view), revealing hexagonal prism shape of the nanorods with planar ends. (b) Side-view SEM image. (c) TEM image taken on the top end of a single nanorod, the six crystallographic planes on the top end are contoured in white dashed line for clarity. The inset is its corresponding SAED pattern, revealing single crystalline nature of the ZnO nanorod with [0001] orientation. (d) TEM image taken on the root sections of the ZnO nanorods.

each other with internal angles about 120°. A side-view (Figure 1b) shows that the nanorods are about 10 μm long with equal diameters of 500 nm from bottom to top of the rods. TEM observation (Figure 1c) on the top end of a single ZnO nanorod confirms that the nanorod is a normal hexagonal prism in shape, and the selected area electron diffraction (SAED) pattern (lower-right inset of Figure 1c) taken from the nanorod indicates that the nanorod is single-crystal and grows along [0001] orientation. TEM observation on the root sections of the ZnO nanorods (Figure 1d) displays that the nanorods have cone-shaped roots, which serve as the groundwork of the nanorods.

Our experiments reveal that the morphology and size of the resultant ZnO nanorods could be tuned by adjusting (i) the concentration of $Zn(NH_3)_4^{2+}$ complex ions in the electrolyte, (ii) the electrodeposition duration, and (iii) the applied current density. The diameters of the ZnO nanorods could be tuned by the concentration of $Zn(NH_3)_4^{2+}$ complex ions in the electrolyte. From parts a−d of Figure 2, it can be observed that the diameters of the ZnO nanorods increase with $Zn(NH_3)_4^{2+}$ concentration under the same applied current density. XRD measurements reveal that there only exists one main peak of (002) for smaller diameter ZnO nanorods (see Figure S2a of Supporting Information). However, with the diameter increase of the ZnO nanorods, there appear more peaks of (100), (101), (102), and (110) (see Figure S2b of Supporting Information), which can be attributed to the increase of radial crystalline size of the nanorods.

The lengths of the ZnO nanorods can be tailored by tuning the electrodeposition duration. Our experiments reveal that the resultant nanorods become longer and longer with the increase of the electrodeposition duration, while the diameter of the nanorods varies little along the *a*-axis (see Figure S3 of Supporting Information). This can be ascribed to the continuous dissolution of the Zn anode to form Zn^{2+} ions in the solution, resulting in a dynamic equilibrium for $Zn(NH_3)_4^{2+}$ concentration, which ensures the sequential growth of the ZnO nanorods.

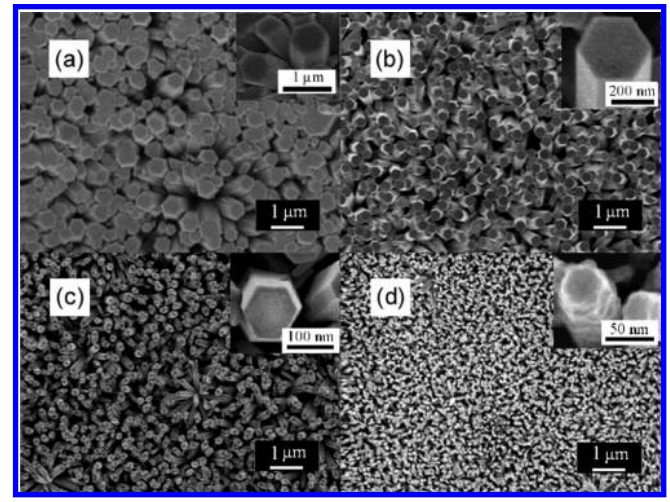

Figure 2. Top-view SEM images of the ZnO nanorods electrodeposited under a constant current density of 0.8 mA cm^{-2} for 10 h at 80 °C in electrolytes with different $Zn(NH_3)_4(NO_3)_2$ concentrations of 1 M (a), 0.2 M (b), 0.1 M (c), and 0.05 M (d), respectively. The insets are the corresponding close-up views, showing that the nanorods have planar ends. The average diameters of the nanorods in a−d are about 800, 200, 100, and 50 nm, respectively.

The applied current density in the electrodeposition is another crucial parameter influencing the morphology of ZnO nanorods. It is well-known that the electric field has four effects on the growth of the ZnO nanorods, i.e., separating Zn^{2+} from Zn anode, deoxidizing NH_3 to generate OH^- near the cathode, inducing dominant growth direction of ZnO nanorods, and affecting the surface energy difference between polar surface ± {0001} and nonpolar surfaces around the side of the nanorods.[26] Our experiments (see Figure S4 of Supporting Information) reveal that the ZnO nanorods can only be achieved under a current density ranging from 0.2 to 3.0 mA cm^{-2}. At low current density (0.01 mA cm^{-2}), ZnO film consisting of nanoparticles has been obtained (Figure S4a of Supporting Information). In this case, ZnO grow freely along the *c* axis under the weak electric field. As the current density is increased to 0.2−3.0 mA cm^{-2}, the ZnO growth direction is dominated along the electric field and the nanorods are achieved (see Figure S4b of Supporting Information). If the current density is increased further to 5.0 mA cm^{-2}, the growth of the nanorods along the *a*-axis becomes obvious, thus ZnO nanorods are conglutinated together (see Figure S4c of Supporting Information). The connected tops of the ZnO nanorods can be clearly observed. When the current density is too high (more than 30 mA cm^{-2}), the products are randomly distributed ZnO stacks (see Figure S4d of Supporting Information). As high current density would disturb the difference of surface energy, leading to quick dissolution of Zn anode to form Zn^{2+} ions in the solution. Thus, higher concentration of Zn^{2+} ions will result in their combination with OH^- to form $Zn(OH)_2$, which gradually accumulates on the substrate and ZnO stacks are formed. XRD spectra of the nanostructures (the right panels of see Figure S4 of Supporting Information) clearly show obvious change of the growth direction from the *c*-axis to *a*-axis with the increase of the current density.

On the basis of all the above-mentioned results, we propose a reasonable formation mechanism for the aligned ZnO nanorods with planar ends as follows. When the Zn sheet (as anode) and the *n*-Si substrate (as cathode) are dipped into $Zn(NH_3)_4(NO_3)_2$ electrolyte, the element Zn on the anode will dissolve into the solution to form Zn^{2+} ions after a suitable electric field is

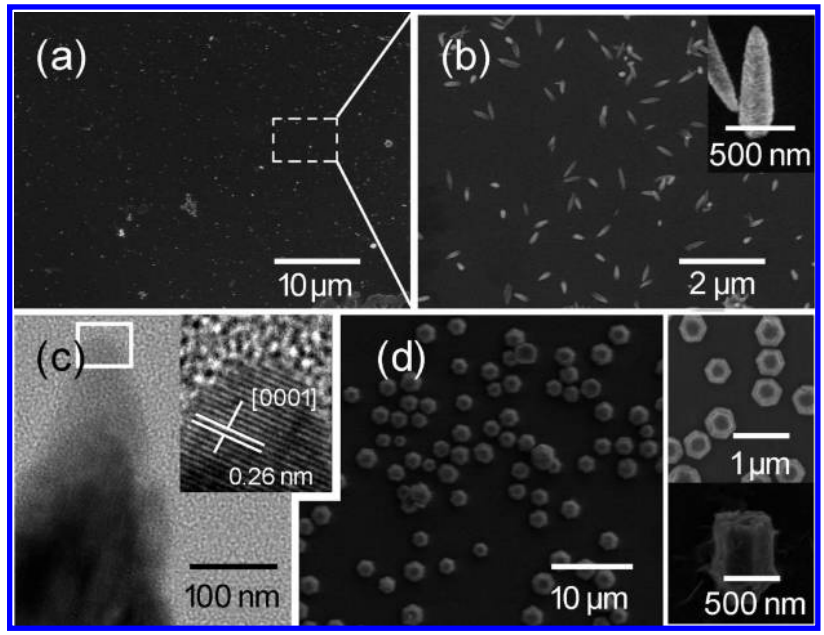

Figure 3. Lower (a) and higher (b) magnification SEM images of the seed layer electrodeposited from 0.5 M $Zn(NH_3)_4(NO_3)_2$ electrolyte. The inset of b is a close-up view of the self-formed seeds. (c) HRTEM image taken on the top of an individual seed. The inset is the lattice-resolved image taken from the square region marked in white. (d) SEM image of the seed layer electrodeposited from 1 M $Zn(NH_3)_4(NO_3)_2$ electrolyte. The upper- and lower-right insets are the close-up top- and side-views, respectively.

applied, leading to the release of two electrons. Zn^{2+} ions in the electrolyte will move to the Si cathode under the applied electric field. Because of the high negative reduction potential ($E_0 = -0.7618$ V) of the Zn^{2+} ions,[27] they are not easily reduced to Zn atoms but attract OH^- ions deoxidized by NH_3 to form $Zn(OH)_2$, which gradually dehydrates into ZnO at 80 °C. The overall reactions for the formation of the ZnO nanorods are given as follows.[28]

$$Zn \rightarrow Zn^{2+} + 2e$$

$$Zn(NH_3)_4(NO_3)_2 \rightarrow Zn(NH_3)_4^{2+} + 2NO_3^-$$

$$Zn(NH_3)_4^{2+} \leftrightarrow Zn^{2+} + 4NH_3$$

$$NH_3 + 3H_2O + 2e \rightarrow NH_4^+ + 3OH^- + H_2\uparrow$$

$$Zn^{2+} + 2OH^- \rightarrow Zn(OH)_2 \xrightarrow{<335K} ZnO + H_2O$$

The formation process of the ZnO nanorods undergoes initial self-nucleation and subsequent growth. The self-formed seed layer plays a crucial role in the growth of the aligned ZnO nanorods.[29] At the very beginning of the electrodeposition, ZnO particles are self-formed on Si substrate to form a seed layer and epitaxially grow up along the *c* axis (parts a and b of Figure 3). High-resolution TEM (HRTEM) image of an individual seed (Figure 3c) reveals the single-crystal nature of the seed. The lattice spacing is measured about 0.26 nm, corresponding to the *d* value of the (002) plane of wurtzite ZnO. The growth direction of the nanorod is perpendicular to this plane, i.e., [0001]. When the electrolyte concentration is increased from 0.5 to 1 M, the shapes of the self-formed ZnO seeds change from cone to hexagon (Figure 3d). This shape transition is attributed to the higher growth speed of the ZnO seeds toward radial direction under higher electrolyte concentration.

Moreover, the crystallinity of the seeds plays an important role in the growth of the vertically aligned ZnO nanorods, which can be controlled by tuning the amount of ammonia used in the preparation of $Zn(NH_3)_4(NO_3)_2$ solution. When small amount of ammonia is added into zinc nitrate hexahydrate [$Zn(NO_3)_2 \cdot 6H_2O$] aqueous solution (pH < 10), there remains polycrystalline $Zn(OH)_2$ microparticles in the solution and the resultant ZnO seeds on the Si substrate are polycrystalline (see Figure S5 of Supporting Information). Then, the seeds grow into clusters that finally lead to the formation of fascicled ZnO nanorods. When an appropriate amount of ammonia is added slowly, $Zn(OH)_2$ microparticles will disappear and gradually convert into $Zn(NH_3)_4^{2+}$. We stopped dropping ammonia when the pH value of the solution was about 10. By use of this solution as electrolyte in the electrodeposition, the resultant ZnO seeds are single-crystal and vertically aligned ZnO nanorods can be achieved, as shown in Figure 1. Schematics of wurtzitic ZnO structure and the growth process of the ZnO nanorods are shown in Figure 4. It is well known that the ZnO structure is composed of two interpenetrating tetrahedral sublattices (Figure 4a),[30] and each sublattice includes four atoms per unit cell, and every atom of Zn is surrounded by four atoms of O, or vice versa, which are coordinated at the edges of a tetrahedron. Because of the layered arrangements of the tetrahedrons along the *c*-axis of ZnO, the formed nanorods have planar ends. The ZnO nanorods have equal diameters from the bottom to top due to the dynamic equilibrium of the electrolyte concentration caused by the continuous electro dissolution of the Zn anode to form Zn^{2+} ions in the solution. Taken together, the growth process of the ZnO nanorods includes two steps (Figure 4b): first, ZnO seeds are self-nucleated in the initial stage of the electrodeposition; then the continuous epitaxy on the seeds leads to the growth of ZnO nanorods.

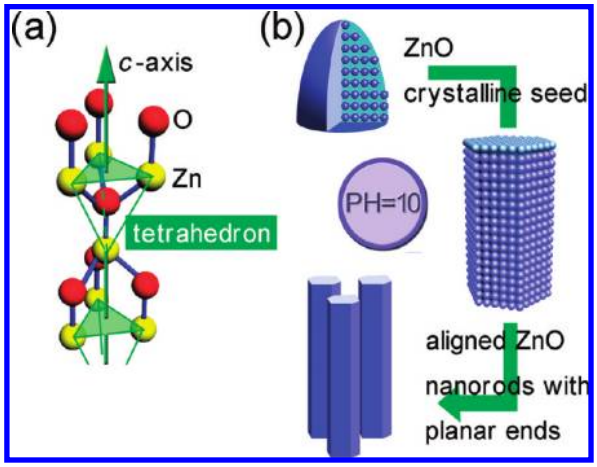

Figure 4. Schematics of (a) the wurtzitic ZnO structure having layered Zn (or O) tetrahedrons along the *c* axis and (b) the growth process of aligned ZnO nanorods.

4. FE Properties

In comparison to conventional thermionic emitters, nanostructured field emitters having good power efficiency and reduction in device size are of great commercial interest in flat panel displays and other electronic devices.[31] It is well-known that the FE properties depend on the ratio of length to diameter (*h*/*r*) of 1D nanostructures;[32] thus we investigated the FE properties of the as-synthesized ZnO nanorods with the same length but different diameters. FE properties were measured in a vacuum chamber under a pressure about 6×10^{-5} Pa at room temperature. The distance between anode and cathode was about 0.100 mm. A 1.084 MΩ resistor was serially connected in the circuit. A direct current voltage ranging from 0.0 to 3.5 kV was applied by a step of 100 V. Figure 5a shows the relationship between the emission current density and the applied electric field (*JE*) for arrays of ZnO nanorods with diameters of ∼200, ∼300, ∼400, and ∼500 nm, respectively, which are determined from the plot curves of the FE currents (*I*) vs the applied voltages (*V*) (see Figure S6 of Supporting Information). The insets in Figure 5a are the top views of four kinds of the ZnO nanorods. The effective emitting areas (marked with red arrows) of these nanorods are 0.839, 0.801, 0.743, and 0.780 cm^2, respectively. The turn-on fields (defined as the applied field of 10 $\mu A\ cm^{-2}$) increase with the nanorod diameters. For the nanorods with diameters of ∼200, ∼300, ∼400, and ∼500 nm, the turn-on fields are about 7.87, 8.87, 10.41, and 12.5 V μm^{-1}, respectively, indicating that under the same electric field, the nanorods with larger diameters exhibit lower current densities. Figure 5b is the corresponding Fowler−Nordheim (F−N) plots with $\ln(J/E^2)$ and $1/E$, showing linear curves for the four samples. The FE is related to the field enhancement factor β and the work function of the emitting material φ, as indicated in F−N formula[33]

$$J = \frac{A\beta^2E^2}{\phi}\exp\left(-\frac{B\phi^{3/2}}{\beta E}\right)$$

Where *J* is the FE current density (A cm^{-2}), *E* is the applied field (V μm^{-1}), *A* and *B* are constants with values of 1.56×10^{-10} A V^{-2} eV and 6.83×10^3 V $eV^{-3/2}$ μm^{-1}, respectively. From the F−N formula, it can be concluded that the slope (*S*) of the $\ln(J/E^2)$ vs $1/E$ plot is proportional to $\varphi^{3/2}$ and inversely proportional to β. As the work function of *n*-type ZnO without doping is generally taken as 5.3 eV,[34] therefore, using the formula $S = -B\varphi^{3/2}/\beta$, the β values of ZnO nanorods with diameters of ∼200, ∼300, ∼400, and ∼500 nm are calculated to be 1429.70, 1307.23, 1204.73, and 1134.91, respectively. It can be concluded that the field enhancement factor increases with the decrease of the rod diameters, further confirming that the ZnO nanorods with smaller diameters have stronger FE capabilities. These well-aligned ZnO nanorods with tunable size and FE properties could have potentials in FE displays and other vacuum microelectronic devices.

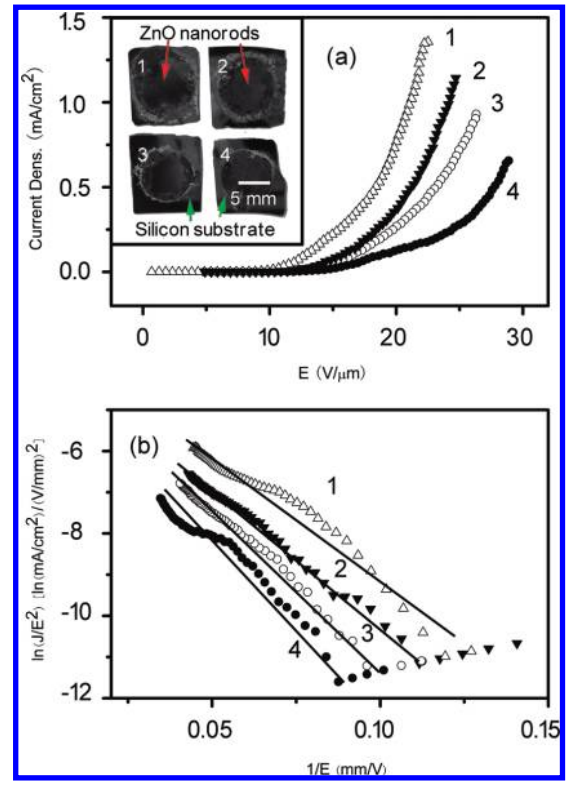

Figure 5. (a) Current density (*J*) as a function of the applied electric field (*E*) curves for ZnO nanorod arrays with diameters of ∼200 nm (curve 1), ∼300 nm (curve 2), ∼400 nm (curve 3), and ∼500 nm (curve 4), respectively. The insets are top views of four kinds of the ZnO nanorod arrays on silicon substrate (green arrows) with different effective emitting areas marked with red arrows. (b) The corresponding F−N plots.

5. Conclusion

In summary, we have developed a very simple electrochemical deposition method for large-scale aligned ZnO hexagonal nanorods with planar ends, without the assistance of any oxidant, seed crystal, or coating of metal oxide layers. The ZnO nanorods grow from initially self-formed single-crystal seeds. The diameters and the lengths of the nanorods can be tuned by controlling the concentration of $Zn(NH_3)_4^{2+}$ complex ions in the electrolyte and the electrodeposition duration, respectively. The ZnO nanorods with smaller diameters exhibit FE properties with higher current densities. The large-area aligned ZnO hexagonal nanorods with planar ends on Si substrate might have potential applications in nanodevices and nanotechnology.

Acknowledgment. We thank financial supports from the National Natural Science Foundation of China (Grant Nos. 50525207, 50972145, 20525312, and 20471028), the National Basic Research Program of China (Grant No. 2007CB936601), and MOE (NCET-04-0449).

Supporting Information Available: The schematic setup for the electrodeposition of ZnO nanorods, XRD measurements on ZnO nanorods with different diameters, ZnO nanorods achieved with different electrodeposition durations, ZnO nanostructures electrodeposited under different current densities, formation process of fascicled ZnO nanorods, and the plot curves of the FE currents (I) vs the applied voltages (V) for the ZnO nanorod arrays with different diameters. This material is available free of charge via the Internet at http://pubs.acs.org.

References and Notes

(1) Wang, X. D.; Song, J. H.; Liu, J.; Wang, Z. L. *Science* **2007**, *316*, 102.

(2) Lu, M.-P.; Song, J. H.; Lu, M.-Y.; Chen, M.-T.; Gao, Y. F.; Chen, L.-J.; Wang, Z. L. *Nano Lett.* **2009**, *9*, 1223.

(3) Huang, M. H.; Mao, S.; Feick, H.; Yan, H. Q.; Wu, Y. Y.; Kind, H.; Weber, E.; Russo, R.; Yang, P. D. *Science* **2001**, *292*, 1897.

(4) Sun, X. W.; Huang, J. Z.; Wang, J. X.; Xu, Z. *Nano Lett.* **2008**, *8*, 1219.

(5) Son, D. K.; You, C. H.; Kim, W. T.; Kim, T. W. *Nanotech.* **2009**, *20*, 365206.

(6) Comini, E.; Faglia, G.; Sberveglieri, G.; Pan, Z. W.; Wang, Z. L. *Appl. Phys. Lett.* **2002**, *81*, 1869.

(7) Shen, G. Z.; Bando, Y.; Liu, B. D.; Golberg, D.; Lee, C. J. *Adv. Fun. Mater.* **2006**, *16*, 410.

(8) Li, C.; Hou, K.; Lei, W.; Zhang, X. B.; Wang, B. P.; Sun, X. W. *Appl. Phys. Lett.* **2007**, *91*, 163502.

(9) Liu, S. C.; Wu, J. J. *J. Mater. Chem.* **2002**, *12*, 3125.

(10) Liu, J. G.; Zhang, Z. G.; Su, X.; Zhao, Y. *J. Phys. D: Appl. Phys.* **2005**, *38*, 1068.

(11) Ye, J. D.; Gu, S. L.; Liu, W.; Zhu, S. M.; Zhang, R.; Shi, Y.; Zheng, Y. D.; Sun, X. W.; Lo, G. Q.; Kwong, D. L. *Appl. Phys. Lett.* **2007**, *90*, 174107.

(12) Shan, C. X.; Liu, Z.; Zhang, Z. Z.; Shen, D. Z.; Hark, S. K. *J. Phys. Chem. B* **2006**, *110*, 11176.

(13) Kim, H. S.; Lugo, F.; Pearton, S. J.; Norton, D. P.; Wang, Y. L.; Ren, F. *Appl. Phys. Lett.* **2008**, *92*, 112108.

(14) Wang, J. M.; Gao, L. *J. Mater. Chem.* **2003**, *10*, 2551.

(15) Li, Y.; Meng, G. W.; Zhang, L. D. *Appl. Phys. Lett.* **2002**, *76*, 2011.

(16) Dobkin, D. M.; Zuraw, M. K. *Principles of Chemical Vapor Deposition*; Springer, 2003.

(17) Rajamathi, M.; Seshadri, R. *Curr. Opin. Solid State Mater. Sci.* **2002**, *6*, 337.

(18) Hsu, Y. F.; Xi, Y. Y.; Tam, K. H.; Djurisic, A. B.; Luo, J. M.; Ling, C. C.; Cheung, C. K.; Ng, A. M. C.; Chan, W. K.; Deng, X.; Beling, C. D.; Fung, S.; Cheah, K. W.; Fong, P. W. K.; Surya, C. C. *Adv. Fun. Mater.* **2008**, *18*, 1020.

(19) Jung, S. H.; Oh, E.; Lee, K. H.; Park, W. J.; Jeong, S. H. *Adv. Mater.* **2007**, *19*, 749.

(20) Liu, B.; Zeng, H. C. *J. Am. Chem. Soc.* **2003**, *125*, 4430.

(21) Li, L.; Pan, S. S.; Dou, X. C.; Zhu, Y. G.; Huang, X. H.; Yang, Y. W.; Li, G. H.; Zhang, L. D. *J. Phys. Chem. C* **2007**, *111*, 7288.

(22) Park, S. K.; Lee, Y. K.; Kwak, H. T.; Park, C. R.; Park, J.; Do, Y. R. *J. Phys. Chem. C* **2008**, *112*, 4129.

(23) Elias, J.; Tena-Zaera, R.; Levy-Clement, C. *J. Phys. Chem. C* **2008**, *112*, 5736.

(24) Wei, Y. G.; Ding, Y.; Li, C.; Xu, S.; Ryo, J.-H.; Dupuis, R.; Sood, A. K.; Polla, D. L.; Wang, Z. L. *J. Phys. Chem. C* **2008**, *112*, 18935.

(25) Zhao, Q.; Xu, X. Y.; Song, X. F.; Zhang, X. Z.; Yu, D. P.; Li, C. P.; Guo, L. *Appl. Phys. Lett.* **2006**, *88*, 033102.

(26) Illy, B.; Shollock, B. A.; M-Driscoll, J. L.; Ryan, M. P. *Nanotechnology* **2005**, *16*, 320.

(27) Matsushita, M.; Sano, M.; Hayakawa, Y.; Honjo, H.; Sawada, Y. *Phys. Rev. Lett.* **1984**, *53*, 286.

(28) Izaki, M. *J. Electrochem. Soc.* **1999**, *146*, 4517.

(29) Kwon, S. J.; Park, J. H.; Park, J. G. *Appl. Phys. Lett.* **2005**, *87*, 133112.

(30) Kisi, E.; Elcombe, M. M.; Crystallogr, A. *Cryst. Struct. Commun.* **1989**, *C45*, 1867.

(31) Jiang, H.; Hu, J. Q.; Gu, F.; Li, C. Z. *Nanotech.* **2009**, *20*, 055706.

(32) Ye, C. H.; Bando, Y.; Fang, X. S.; Shen, G. Z.; Golberg, D. *J. Phys. Chem. C* **2007**, *111*, 12673.

(33) Gadzuk, J. W.; Plummer, E. W. *Rev. Mod. Phys.* **1973**, *45*, 487.

(34) Minami, T.; Miyata, T.; Yamamoto, T. *Surf. Coat. Technol.* **1998**, *108*, 583.

JP9087223